

Parameter mapping between the microscopic nonlocal Nambu–Jona-Lasinio and constant-sound-speed models

S. Antić,^{1,2,*} M. Shahrbafe,¹ D. Blaschke,^{1,3,4} and A. G. Grunfeld^{5,6}

¹*Institute for Theoretical Physics, University of Wrocław, Max Born Pl. 9, 50-204, Wrocław, Poland*

^{2*}*Physics Department, Faculty of Science, University of Zagreb, Bijenička cesta 32, 10000 Zagreb, Croatia*

³*Bogoliubov Laboratory of Theoretical Physics, Joint Institute for Nuclear research, Joliot-Curie str. 6, 141980 Dubna, Russia*

⁴*National Research Nuclear University (MEPhI), Kashirskoe Shosse 31, 115409 Moscow, Russia*

⁵*CONICET, Godoy Cruz 2290, Buenos Aires, Argentina*

⁶*Departamento de Física, Comisión Nacional de Energía Atómica,
Av. Libertador 8250, (1429) Buenos Aires, Argentina*

(Dated: May 4, 2021)

A covariant nonlocal Nambu–Jona–Lasinio (nNJL) model, used to describe the color superconducting quark matter phase in hybrid neutron stars, is parametrized with two free parameters, the dimensionless vector and diquark coupling strengths η_V and η_D . Changing the values of these parameters results in different equations of state (EoS) with varying stiffness. On the other hand, the constant-sound-speed (CSS) model is a frequently used, simple quark matter equation of state with three parameters: the slope parameter A , the speed of sound c_s and the bag pressure B . We show that the CSS model EoS provides an excellent fit to that of the nNJL model. This work provides a simple functional form for the mapping between the parameter spaces of these two models, i.e. the $\eta_D - \eta_V$ and $A - c_s^2 - B$ parameter sets. These results allow for a simplified description of the quark matter phase in neutron stars and for an interpretation of hybrid neutron star phenomenology in terms of parameters of a Lagrangian quark matter model.

I. INTRODUCTION

Recent investigations of neutron star (NS) properties support the idea that deconfined quark matter builds the cores not only of the heaviest known NSs [1], but even of all NSs in the presently observed mass range [2].

In order to draw such conclusions, the equation of state (EoS) for the quark matter phase in NSs is needed. The best candidates to provide a reliable quark matter EoS under neutron star conditions are those effective models that share key features with low-energy QCD, such as dynamical chiral symmetry breaking and the resulting low-energy theorems as the Gell-Mann–Oakes–Renner and Goldberger–Treiman relations. The most popular chiral effective model that reasonably fulfills these requirements is the Nambu–Jona-Lasinio (NJL) model [3, 4], that was developed in order to understand the generation of a mass gap for fermions (nucleons) in analogy to the energy gap in the BCS model of electronic superconductivity, based on local four-fermion interactions. With the introduction of quarks as the fundamental fermionic degrees of freedom of strongly interacting matter, the model has been

reformulated on that level of description, see [5–11] for early reviews and [12] for the NJL model analysis of dense quark matter.

The local NJL-type models have a major caveat: the absence of confinement. A local four-fermion coupling is incompatible with the strong coupling at large-distances that is phenomenologically established by hadron spectroscopy and lattice QCD simulations of the free (potential) energy between static (heavy) color charges that exhibits a funnel-shaped interquark potential. One way to bring effective low-energy QCD models closer to capturing also the confining nature of the strong interaction at large distances is the generalization of the local four-fermion coupling to a nonlocal four-point function. A first step in this direction has been done with so-called “bilocal QCD” models [13, 14] which could successfully address low-energy QCD and hadron phenomenology on the basis of a nonperturbative model gluon propagator [15] or a relativistic generalization of confining potential models [16].

The next step towards the modern formulation of the nonlocal chiral quark model (in the following denoted as “nNJL”) was to generalize the interaction model from a two-point function to a four-point function, following two schemes. The first one defines the nonlocal interac-

* Guest scientist

tion similar to the relativistic S-matrix with its dependence on the kinematic Mandelstam variables and assumes separability (a product ansatz) of pairwise relative momenta [17]. This scheme has later been denoted as one-gluon exchange (OGE) model. For the model formfactors the ansatz has been made of instantaneous (energy-independent) functions that depend on the relative three-momenta only. In this way, the evaluation of thermodynamic properties of the model within the imaginary time formalism became straightforward because the Matsubara summations could still be performed analytically as in the original NJL model which was recovered for a step function as the formfactor. Using smooth functions as formfactors of the nonlocality resulted in a lowering of the pseudocritical temperature of the chiral restoration, closer to the results from lattice QCD [17]. The second scheme, denoted as instanton-liquid model (ILM), was built using a simple product ansatz for the formfactors that were attached to each of the four fermion "legs" [18]. A comprehensive overview over the nonlocal chiral quark models in this early era has been given by Georges Ripka in his book [19], where formal details and more references can be found.

With the extension to rank-2 separable gluon propagator models, and using formfactors depending on the 4-momentum, a close correspondence to the Dyson-Schwinger equation approach could be established [20]. The finite-temperature extension led to a dramatic reduction of the chiral restoration temperature [21] which recently has been found in lattice QCD simulations as $T_c^0 = 132_{-6}^{+3}$ MeV in the chiral limit [22]. When coupling the nonlocal chiral quark dynamics to a gluon background field within the Polyakov-loop extension of the model (see [23] for the details in case of the local NJL model, where besides adding gluonic degrees of freedom at finite temperatures confinement is mimicked), acceptable values and systematics for the pseudocritical temperature of QCD could be obtained [24, 25] and thermodynamic instabilities associated with complex-conjugated mass poles could be largely cured [26].

Another advantage of using covariant formfactors in the nNJL model is that the momentum dependence of the quark mass as well as the wave function renormalization factor of the quark propagator can be described in accordance with lattice QCD simulations [27]. Since the nonperturbative low-energy interaction of the nNJL model can be calibrated using lattice QCD simulations, one has a serious basis to extend studies of thermo-

dynamic properties from the temperature axis into the whole phase diagram including high baryochemical potentials where no lattice QCD simulations are available because of the severe sign problem. Using the nNJL model with realistic formfactors, the position of the critical endpoint in the phase diagram has been obtained for temperatures below 130 MeV [28, 29], a prediction that can be investigated in the upcoming heavy-ion collision experiments with collision energies $\sqrt{s_{NN}} \sim 3 - 6$ GeV, e.g., at the NICA facility of JINR Dubna, or in the fixed-target experiment at RHIC, see Fig. 14 of Ref. [30]. A recent detailed review on nNJL models and their applications to studies of matter under extreme conditions is given in [31].

In the present work we want to study the EoS of quark matter in NSs at vanishing temperature. A first application of the covariant nNJL model has been given in [32], where a simple Gaussian formfactor was used and only the scalar-pseudoscalar meson interaction channel has been included. It could be shown that such a model with two quark flavors is equivalent to a thermodynamic bag model with a bag pressure $B = 81.3$ MeV/fm³. The strange quark flavor appeared sequentially at a higher density and rendered the corresponding neutron star unstable against gravitational collapse for masses above $1.62 M_\odot$. In order to describe stars with masses above $2 M_\odot$ as required by recent neutron star observations [33], one has to include a repulsive vector meson interaction channel¹. In hybrid star models the transition to such a quark matter phase occurs only at rather high densities, close to the maximum mass of the sequence. As it is known from studies using the local NJL model, the simultaneous addition of a scalar diquark interaction channel leads to the effect of diquark condensation (color superconductivity) which pushes the onset of quark deconfinement to lower densities and results in quark matter cores for neutron stars with typical masses of $\sim 1.4 M_\odot$ [35, 36]. The situation is similar for the covariant nNJL model where increasing the diquark coupling results in a lowering of the onset density for the chiral restoration transition [37]. Correspondingly, a phenomenologically satisfactory situation occurs for the hybrid neutron star EoS when a repulsive vector and diquark interaction channel is included to the covariant nNJL model [38] since it develops an early deconfinement

¹ We note that in the local limit such a model has been introduced as "vBag model" [34].

transition to a stiff color superconducting quark matter phase.

Consequently, we will use in this study the covariant nLNL model in the OGE scheme that is parameterized with the dimensionless vector and diquark coupling strengths (η_V and η_D), given as ratios of the vector and diquark couplings, G_V and G_D , to the scalar coupling constant G_S , respectively. The values of these input parameters, however, are not known from first principles.

While the original version of the nLNL model is formulated with constant, density-independent coefficients, in Refs. [39, 40] density-dependent coefficients have been introduced in such a way that the results of a recent relativistic density-functional approach to quark matter [41] could be reproduced. The applicability of both versions of nLNL model in constructing the phase transition from hypernuclear matter to deconfined quark matter has also been investigated [42, 43].

The microscopic approach of the nLNL model has the advantage that it allows to relate the spectrum of observable NS properties to the ranges of η_V and η_D parameters in the Lagrangian of an effective low-energy QCD model (for details, see [44]). It involves, however, time-consuming numerical routines for solving the self-consistent nonlocal mean field equations together with an extrapolation procedure at high densities. For this reason, we explore the possibility to mimic the nLNL results with simpler approach, the constant-sound-speed (CSS) model [45, 46].

The CSS approach is widely used in the literature, in particular, for the classification [45] and systematics [47, 48] of hybrid neutron stars. Among the applications of the CSS model is also the investigation of the third and fourth families of compact stars for which stable branches have been verified as well [49–51]. The work of Ref. [46] demonstrates the possibility for NJL model-based approaches to color-superconducting cold quark matter to be well approximated by CSS parameterization. It was shown that the EoS for quark matter developed for the nonlocal separable NJL model with formfactors depending on the three-momentum in [52, 53] can be well fitted with the CSS model.

It is also worth mentioning that the CSS extrapolation becomes necessary for nLNL models of certain values of η_V and η_D parameters due to the limitation of its covariant formfactor realization [37] to chemical potentials up to ~ 1600 MeV. However, we would like to map the nLNL EoS to the CSS EoS for the whole range of

chemical potentials in the quark matter phase, and not only for $\mu_B > 1600$ MeV, as it was previously done [44]. This mapping would enable a replacement of the complicated quark matter EoS by a simple model which gives the EoS of quark matter not only in the two-flavor color-superconducting (2SC) phase but also at higher densities for the color-flavor-locked (CFL) phase.

The main idea of this work is to provide a simple functional form that enables a mapping between the two parameter spaces, the nLNL model parameters η_V and η_D and the parameters of the CSS model: the slope parameter A , the squared speed of sound c_s^2 and the bag pressure B . With the simplified description of the quark phase in hybrid NSs, its EoS would become easier to handle and would at the same time have strong microphysical justification.

The structure of the present paper is as follows: in Sec. II we introduce the formulations of both nLNL and CSS models and their parameters, along with an additional phenomenological EoS of Alford [54] for comparison. In Sec. III the functional dependence between the two parameter sets is found and parameter mapping between the two models is discussed. Finally, the main conclusion are given in Sec. IV.

II. EQUATION OF STATE MODELS FOR THE QUARK MATTER PHASE OF A NEUTRON STAR

A. Generalized nLNL model with η_V and η_D parameters

For the microphysical description of the quark matter phase we consider a chiral quark model that includes nonlocal separable interactions and can be considered as a nonlocal extension of the NJL model (nLNL). We employ the two-flavor $SU(2)_f$ model, developed in Refs. [17, 37, 38], that is described by the Lagrangian

$$\mathcal{L} = \bar{\psi}(-i\cancel{\partial} + m_c)\psi - \frac{G_S}{2}j_S^f j_S^f - \frac{G_D}{2}[j_D^a]^\dagger j_D^a + \frac{G_V}{2}j_V^\mu j_V^\mu, \quad (1)$$

with the nonlocal generalizations of the quark currents

$$j_S^f(x) = \int d^4z g(z)\bar{\psi}(x + \frac{z}{2})\Gamma^f\psi(x - \frac{z}{2}), \quad (2)$$

$$j_D^a(x) = \int d^4z g(z)\bar{\psi}_C(x + \frac{z}{2})i\gamma_5\tau_2\lambda^a\psi(x - \frac{z}{2}), \quad (3)$$

$$j_V^\mu(x) = \int d^4z g(z)\bar{\psi}(x + \frac{z}{2})i\gamma_\mu\psi(x - \frac{z}{2}), \quad (4)$$

in the scalar meson, scalar diquark and vector meson channels, respectively. The grand canonical partition function of the quark matter system,

$$\mathcal{Z} = \int \mathcal{D}\bar{\psi}\mathcal{D}\psi \exp \left\{ - \int_0^\beta d\tau \int d^3x [\mathcal{L} - \mu\bar{\psi}\gamma_0\psi] \right\}, \quad (5)$$

after bosonization by the Hubbard-Stratonovich transformation, can be evaluated in the mean field approximation (MFA) with the result for the thermodynamical potential

$$\begin{aligned} \Omega^{\text{MFA}} &= -T \ln \mathcal{Z}^{\text{MFA}} \\ &= \frac{\bar{\sigma}^2}{2G} + \frac{\bar{\Delta}^2}{2H} - \frac{\bar{\omega}^2}{2G_V} \\ &\quad - \frac{1}{2} \int \frac{d^4p}{(2\pi)^4} \ln \det [S^{-1}(\bar{\sigma}, \bar{\Delta}, \bar{\omega}, \mu_{fc})], \end{aligned} \quad (6)$$

see Refs. [37, 38] for details.

The inclusion of the scalar diquark channel together with the repulsive vector interaction channel, plays an important role in the phenomenology of hybrid EoS of compact stars.

The diquark condensate gives rise to color superconductivity (2SC) and is responsible for lowering the onset of the phase transition from the phase with broken chiral symmetry to the 2SC phase. The vector interaction induces a stiffening behaviour in the EoS, that is essential to reach compact stars masses above $2M_\odot$. Systematic investigation of hybrid NS properties reveals [36, 44] that phenomenological constraints from mass and radius measurements are optimally fulfilled when an increase in the diquark coupling is accompanied by a simultaneous increase in the vector coupling.

The model includes three input parameters: m_c (current quark mass), p_0 (effective momentum scale) and G_S (coupling constant). They are determined as to reproduce the pion mass and decay constant as well as the chiral condensate in the vacuum, at vanishing temperature and densities. The two remaining coupling constants G_S and G_V are driving the terms that, after bosonization, give rise to the color superconducting gap and the vector meson mean field. The dimensionless ratios $\eta_D = G_D/G_S$ and $\eta_V = G_V/G_S$ are free parameters. From a Fierz rearrangement of the OGE interactions one obtains $\eta_D = 3/4$ and $\eta_V = 1/2$ that could serve as an orientation for the values of these parameters in the vacuum. There is no precise derivation of effective couplings from QCD, as we consider here the strongly nonperturbative low-energy regime. Moreover,

one has to expect that these couplings could be subject to a medium dependence. However, η_D values larger than $\eta_D^* = (3/2)m/(m - m_c)$ may lead to color symmetry breaking in the vacuum [55] (where m stands for the dressed mass and m_c for the current quark mass).

In the present work we consider a window of values for η_D and η_V that was also explored in previous works Ref. [36, 39, 56].

The mean field values $\bar{\sigma}$, $\bar{\Delta}$ and $\bar{\omega}$ are obtained from the coupled equations

$$\frac{\partial \Omega^{\text{MFA}}}{\partial \bar{\sigma}} = 0, \quad \frac{\partial \Omega^{\text{MFA}}}{\partial \bar{\Delta}} = 0, \quad \frac{\partial \Omega^{\text{MFA}}}{\partial \bar{\omega}} = 0. \quad (8)$$

As we intend to describe the behaviour of quark matter in the cores of NSs, we have to take into account the presence of leptons (electrons and muons) which we include into the thermodynamic potential as free relativistic Fermi gases. In addition, we have to consider that the stellar matter satisfies the following conditions: equilibrium under weak interactions (chemical equilibrium) as well as color and electric charge neutrality. As a consequence, it can be seen that the six different chemical potentials μ_{fc} (depending on the two quark flavors u and d and quark colors r, g and b) in Eq. (7) are not independent from each other and can be written in terms of three independent quantities: the baryonic chemical potential μ , the electron chemical potential μ_e and a color chemical potential μ_8 . Basically, for each value of μ we solve self-consistently the gap equations (8), complemented with the conditions for β -equilibrium and electric charge and color charge neutrality (details of the calculation can be found in the Appendix of Ref. [38]).

In the present work, we consider a Gaussian form factor $g(p) = \exp(-p^2/p_0^2)$ in Euclidean 4-momentum space. The fixed input parameters of the quark model considered here are $m_c = 5.4869$ MeV, $p_0 = 782.16$ MeV and $G_S p_0^2 = 19.804$.

B. Constant speed of sound formulation

The CSS EoS at zero temperature can be written in the form [45, 47]

$$P(\mu) = A \left(\frac{\mu}{\mu_x} \right)^{1+\beta} - B, \quad (9)$$

where $\mu_x = 1$ GeV defines the scale for chemical potential, A is a slope parameter in the units of the pressure, B is the bag pressure and $\beta = 1/c_s^2$ is a parameter related

to the squared speed of sound $c_s^2 = dP/d\varepsilon$. The pressure as a function of the chemical potential is a thermodynamical potential from which other EoS can be obtained by derivation. For instance, the baryon density reads

$$n_B(\mu) = \frac{dP(\mu)}{d\mu} = A \frac{1+\beta}{\mu_x} \left(\frac{\mu}{\mu_x} \right)^\beta, \quad (10)$$

and the energy density is given by

$$\varepsilon(\mu) = \mu \frac{dP(\mu)}{d\mu} - P(\mu) = A\beta \left(\frac{\mu}{\mu_x} \right)^{1+\beta} + B. \quad (11)$$

Using the definition of the pressure (9), the energy density (11) can be rewritten as

$$\varepsilon(P) = \beta P + (1+\beta)B, \quad (12)$$

which directly reveals that the squared sound speed is $c_s^2 = 1/\beta = \text{const}$, since $\beta = \text{const}$.

The speed of sound determines the stiffness of the EoS, which has to be large enough to allow for the maximum neutron star mass to fulfil the observational lower bound of $2.01 M_\odot$ from the Shapiro-delay based mass measurement on PSR J0740+6620 [33] (a recent upgrade of the former mass measurement [57]) at the 1σ level. The prefactor A changes the slope of the $P(\mu)$ curve and has thus also an effect on the stiffness of the EoS: lowering the value of A increases the stiffness. The effective (negative) bag pressure B realises quark confinement at low densities in quark matter EoS because it makes sure that any small but positive pressure of a hadronic phase would be preferable this region. The parameters A , B and c_s^2 are free parameters which define the behaviour of the quark matter EoS.

It is worth mentioning that for a large class of quark matter models, including the standard NJL model [58, 59] or its nonlocal generalization with instantaneous, three-momentum dependent formfactors [60], it was observed that the sound speed appears largely density-independent [46]. For the covariant nNJL model such an observation has not yet been made. Therefore, for the first time in the present work the question is considered how well the covariant nNJL model in the 2SC phase can be approximated by the quark matter EoS with constant speed of sound, given by Eq. (9).

C. Phenomenological EoS

Besides the CSS model EoS, there is a phenomenological formulation of the EoS of quark matter in use which

has been introduced and motivated in Ref. [54]. In that work, the quark matter EoS consists of the first three terms of a series in even powers of the quark chemical potential

$$\Omega_{QM} = -3/4\pi^2 a_4 \mu^4 + 3/4\pi^2 a_2 \mu^2 + B_{\text{eff}}, \quad (13)$$

where a_4 , a_2 , and B_{eff} are coefficients independent of μ .

The quartic coefficient $a_4 = 1 - c$ is well defined for an ideal massless gas for which $c=0$. Perturbative QCD corrections in lowest order, i.e. $O(\alpha_s)$ for massless quark matter lead to a reduction of a_4 , e.g., accounted for by $c = 0.3$ so that $a_4 = 0.7$. The quadratic μ^2 term arises from an expansion in the finite strange quark mass m_s and the diquark pairing gap Δ , so that $a_2 = m_s^2 - 4\Delta^2$. In CFL quark matter, they are almost in the same order of about 100 MeV so that the coefficient a_2 is almost zero and this corresponds to a constant speed of sound $c_s^2 = 1/3$, the conformal limit [54]. In the phenomenological parameterization (13), the coefficient a_2 usually varies in the limits $\pm(150 \text{ MeV})^2$ [61].

However, this EoS for quark matter is softer than some nucleonic ones. It has been shown in [54] that even for this simple parameterization which hereafter we call "Alford fit", the resulting hybrid stars can have mass-radius relations very similar to those of pure nucleonic stars and the maximum mass fulfills the constraint for its observational lower limit [33].

As another aim of the present work, we intend to compare the results of fitting the nNJL EoS with both CSS parameterization and Alford parameterization.

III. RESULTS AND DISCUSSION

A. Fitting procedure

In order to obtain a functional relation between the parameters of the two approaches, we considered 34 EoS based on nNJL model (for different values of η_D and η_V parameters) to which we fit the CSS EoS (9) in order to obtain the values of A , B and β . In these EoS fits, the parameter B is expressed through the values of A and β as

$$B = A \left(\frac{\mu(P=0)}{\mu_x} \right)^{1+\beta}, \quad (14)$$

with the value of chemical potential for which the pressure is equal to zero, given by the nNJL EoS.

One example of the CSS fit to the nlNJL EoS (with $\eta_D = 0.75$ and $\eta_V = 0.14$) is given in Fig. 1. For comparison, fitting the parameters of the phenomenological EoS (13) that was introduced by Alford et al. in [54] we obtain $a_4 = 0.003$, $a_2 = -(102.342 \text{ MeV})^2$ and $B_{\text{eff}} = 124.53 \text{ MeV fm}^{-3}$. This "Alford fit" is also shown in Fig. 1. It is worth mentioning that the value of $a_4 \approx 0$, which is obtained by the fit, entails that the correction relative to the ideal gas limit is close to 100% and thus not compatible with its value of $c = 2\alpha_s/\pi \approx 30\%$ in perturbation theory to $O(\alpha_s)$ [62]. This can be seen as an hint to the nonperturbative nature of the quark matter EoS in this domain of low chemical potentials in the vicinity of the hadronization transition.

In the inserted plot we further examine the low chemical potential region where the most significant difference between the two fits is found. The CSS follows the nlNJL behaviour more closely, which will be also manifested in the mass-radius curves discussed toward the end of the chapter. For the remaining chemical potentials, the two fits present the same quality in reproducing the nlNJL EoS. The quality of the fits is estimated with the χ^2 value, defined as

$$\chi^2 = \sum_i^N \frac{(P_{\text{nlNJL}}(\mu_i) - P_{\text{fit}}(\mu_i))^2}{\sigma_i^2}, \quad (15)$$

where N is the number of points for the chemical po-

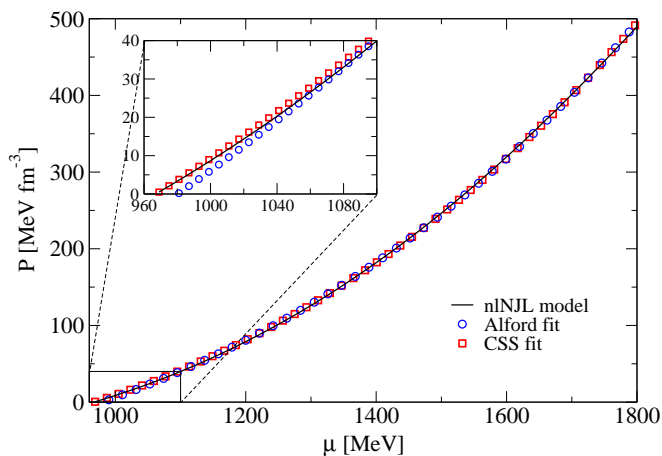


FIG. 1. EoS of the original nlNJL model for the parameter set $(\eta_D, \eta_V) = (0.75, 0.14)$ compared to its fit by the phenomenological form (13) (Alford fit, blue circles) with the parameters $a_4 = 0.003$, $a_2 = -(102.342 \text{ MeV})^2$ and $B_{\text{eff}} = 124.53 \text{ MeV fm}^{-3}$ as well as the fit by the CSS pressure of Eq. (9) (red squares) with the parameters $A = 94.875$, $c_s^2 = 0.481$ and $B = 85.614$, see Tab. I.

model in question defined as $\sigma^2 = \frac{1}{N} \sum_i^N (P_{\text{nlNJL},i} - \bar{P})^2$, where \bar{P} is the mean value of the nlNJL model pressures, $\bar{P} = \frac{1}{N} \sum_i^N P_i$. The $P_{\text{nlNJL}}(\mu_i)$ and $P_{\text{fit}}(\mu_i)$ are the values of pressure in nlNJL model and for the fit in each point of chemical potential μ_i . The χ^2 value for CSS fit is 0.031 while it is 0.038 for Alford's fit.

From the CSS fit, the values of A and β parameters are obtained, from which B parameter and squared speed of sound c_s^2 are calculated. These values are given in Table I together with the χ^2 values for the 34 different nlNJL EoSs giving the total of 34 data points. From these values the functional form, between nlNJL parameter space and the CSS one, is to be found.

In order to find the functional dependence between the two parameter spaces, we analyze the behaviour of the CSS model parameters for different values of η_D and η_V , as given in Figure 2. The parameter A shows the strongest dependence on both nlNJL model parameters, while c_s^2 and B are almost independent on η_D and linearly depending on η_V , respectively. From these dependencies, the simplest functional form between two parameter spaces can be assumed: the variation of CSS parameters is linear with the change of η_D , while it is quadratic with the change of η_V . Thus, we write the following equations

$$A = a_1\eta_D + b_1\eta_V^2 + c_1 \quad (16)$$

$$c_s^2 = a_2\eta_D + b_2\eta_V^2 + c_2 \quad (17)$$

$$B = a_3\eta_D + b_3\eta_V^2 + c_3, \quad (18)$$

where the coefficients a_i , b_i and c_i (with $i = 1, 2, 3$) are obtained through a two-parameter (η_D, η_V) fitting procedure of each of the CSS parameters (A , B , c_s^2) and are given in Table II.

To check the quality of our method, we choose one original nlNJL EoS that was not included in the initial fitting data set (e.g. $\eta_D = 0.75$ and $\eta_V = 0.15$) and calculate CSS EoS using Eq. (9) with the parameter values obtained through Eqs. (16)-(18). The EoS comparison is given in Fig. 3. It is worth noticing that the $M - R$ curve for our example EoS with the parameter set $(\eta_D, \eta_V) = (0.75, 0.15)$ from the middle of the parameter range crosses the revised mass value $2.08 M_\odot$ for PSR J0740+6620 [33] at the radius $R = 12.5 \text{ km}$, which accidentally is in the middle of the overlap region $12.2 \text{ km} < R < 13.7 \text{ km}$ of the 1σ NICER radius measurements from the two analysis teams (Riley et al. and Miller et al.) that have recently been reported [63].

We have performed the fitting procedure considering the Alford parameterization as well. The results show

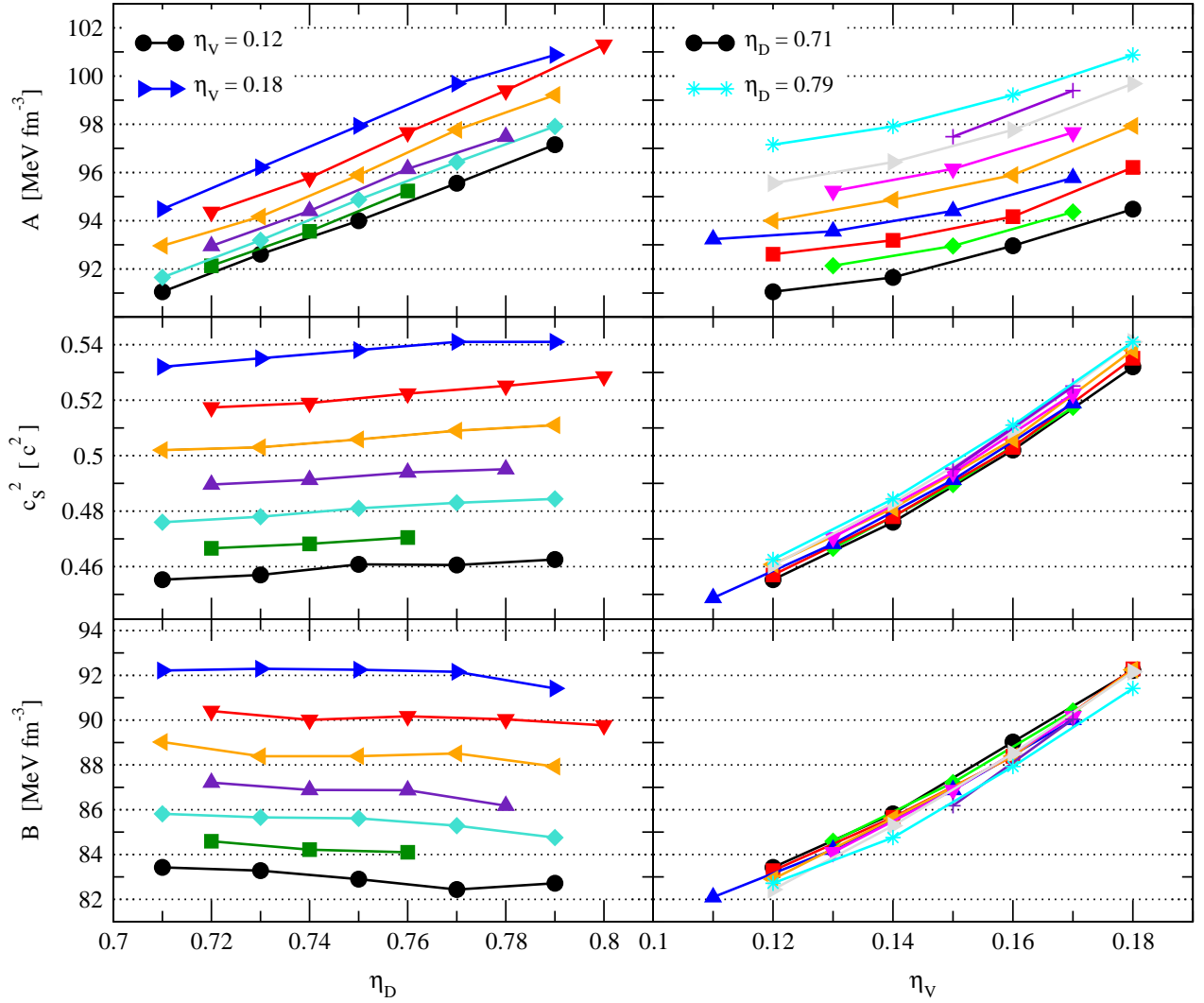


FIG. 2. The change of CSS parameters (A , c_s^2 and B) with the increase of η_D for different values of η_V (from 0.12 to 0.18 in steps of 0.01) on the left panels, and with the increase of η_V for different values of η_D (from 0.71 to 0.78 in steps of 0.01) on the right panels.

that the CSS parameterization works better for fitting the nI NJL model. For comparison, the mass-radius ($M-R$) curves for the hybrid stars constructed using nI NJL model and two different versions of fitted EoS are shown in Fig. 4. For the hadronic EoS we have employed the relativistic density-functional (RDF) model based on the DD2 parameterization [66] with excluded volume effects [67]. The DD2 model with excluded volume is mainly used in the context of an early deconfinement onset with large latent heat.

The results for the $M-R$ curves sufficiently demonstrate the applicability of the mapping that has been performed. It is clear that the $M-R$ curves for the CSS fit and its functional version are sufficiently close

for these two parameterizations to be considered equivalent. Furthermore, their difference to the $M-R$ curve for the original nI NJL EoS amounts to maximally 200 m in radius. This difference is well visible but still much smaller than the design accuracy of observational radius measurements from NICER, which even has not yet been reached by the first NICER radius measurements. Therefore, our work provides a sufficiently precise tool for NS phenomenology. Moreover, the comparison with Alford fit shows that the radius of the NS is really sensitive to the EoS. While both fits are very close according to Fig. 1, the CSS parameterization performs better in the $M-R$ curve, in particular close to the onset of the phase transition at low densities. From our results, we can see

TABLE I. The values of A , B and c_s^2 calculated from the CSS EoS fit to the given nI NJL model defined by the values of η_D and η_V .

η_D	η_V	A [MeV/fm ³]	c_s^2 [c ²]	B [MeV/fm ³]	χ^2
0.70	0.15	91.484	0.488	87.209	0.039
0.71	0.12	91.053	0.4557	83.425	0.022
0.71	0.14	91.649	0.476	85.815	0.032
0.71	0.16	92.963	0.502	89.021	0.047
0.71	0.18	94.481	0.532	92.214	0.075
0.72	0.13	92.132	0.467	84.592	0.026
0.72	0.15	92.954	0.49	87.209	0.038
0.72	0.17	94.366	0.517	90.408	0.058
0.73	0.12	92.612	0.457	83.28	0.021
0.73	0.14	93.19	0.478	85.658	0.031
0.73	0.16	94.17	0.503	88.385	0.048
0.73	0.18	96.211	0.535	92.29	0.073
0.74	0.11	93.236	0.449	82.095	0.017
0.74	0.13	93.563	0.468	84.217	0.026
0.74	0.15	94.41	0.491	86.884	0.039
0.74	0.17	95.78	0.519	90.011	0.061
0.75	0.12	94	0.461	82.899	0.044
0.75	0.14	94.875	0.481	85.614	0.031
0.75	0.16	95.894	0.506	88.391	0.056
0.75	0.18	97.934	0.538	92.249	0.078
0.76	0.13	95.235	0.47	84.101	0.027
0.76	0.15	96.153	0.494	86.873	0.039
0.76	0.17	97.66	0.522	90.172	0.063
0.77	0.12	95.556	0.461	82.437	0.021
0.77	0.14	96.433	0.483	85.287	0.032
0.77	0.16	97.77	0.509	88.512	0.074
0.77	0.18	99.685	0.541	92.155	0.085
0.78	0.15	97.485	0.495	86.179	0.042
0.78	0.17	99.34	0.525	90.034	0.065
0.79	0.12	97.604	0.464	82.718	0.02
0.79	0.14	97.912	0.484	84.755	0.033
0.79	0.16	99.216	0.511	87.929	0.053
0.79	0.18	100.878	0.541	91.415	0.084
0.8	0.17	101.116	0.528	89.766	0.070

that the Alford fit may be useful close to the maximum mass.

We conclude that for the nI NJL EoS parameterizations within the ranges $0.7 < \eta_D < 0.8$ and $0.11 < \eta_V < 0.18$, the CSS approach can mimic the behaviour of the nI NJL EoS to high accuracy. The range of η_D values between 0.7 and 0.8 is covering the value for the Fierz transformation of a one-gluon exchange interaction ($\eta_D = 3/4$) and entails that the quark matter is in the color superconducting phase. The CSS parameters for the nI NJL EoSs

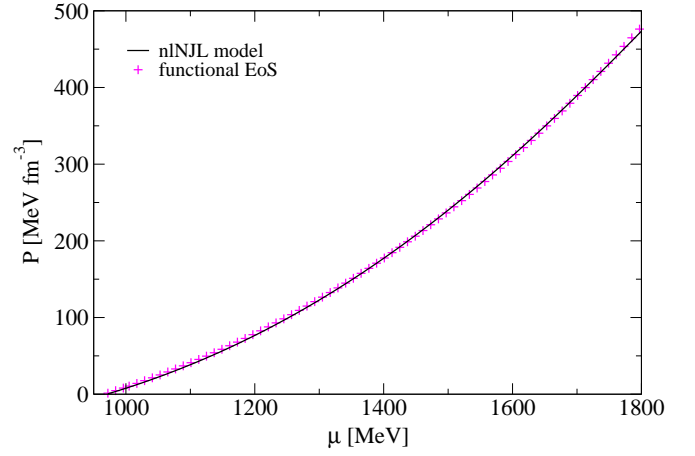


FIG. 3. Comparison of the EoS for the original nI NJL for $\eta_D = 0.75$ and $\eta_V = 0.15$ (black solid line) with its CSS representation (magenta pluses) calculated from Eq. (9) where the parameters $A = 93.586$, $c_s^2 = 0.487$ and $B = 84.454$ are determined using the functions (16)-(18) with the coefficients from Tab. II. The χ^2 value of the fit is 0.049.

with high values of $\eta_V > 0.18$ are showing deviations from the general behaviour fitted by Eqs. (16)-(18). But since for these η_V -values there is a causality violation at large chemical potentials, the CSS form of the EoS fitted at low densities can be used to extrapolate the EoS above a certain density. A lower limit on the values of the η_V parameter is not explored here.

IV. CONCLUSION

We have considered the correspondence between the covariant nI NJL model and the CSS model EoS. We have performed a mapping between the parameters of these two models in a decent range with a χ^2 value that qualifies an excellent fit. The finding of this equivalence allows to employ the simpler CSS approach instead of the covariant nI NJL model when a hybrid star EoS with color superconducting quark matter shall be constructed. The

TABLE II. The values of a_i , b_i and c_i coefficients ($i = 1, 2, 3$) for the mapping between the (η_D, η_V) and (A, c_s^2, B) parameter spaces given by Eqs. (16)-(18).

i	parameter	unit	a_i	b_i	c_i
1	A	MeV fm ⁻³	80.663	199.809	30.575
2	c_s^2	c ²	0.112	4.318	0.312
3	B	MeV fm ⁻³	10.43	-502.998	-83.462

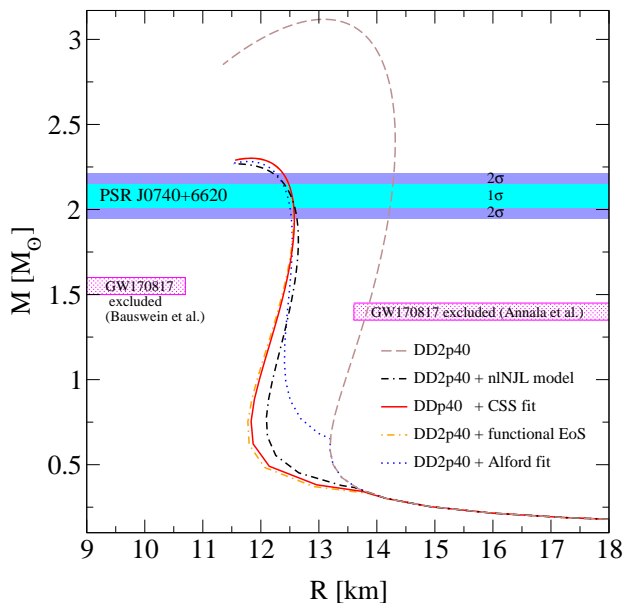


FIG. 4. The $M - R$ sequences for hybrid star EoS obtained by a Maxwell construction for a DD2p40 EoS (brown dashed line) with the nlNJL model (black double dashed dotted line; $\eta_D = 0.75$, $\eta_V = 0.14$), its CSS fit (red solid line), the functional mapping (orange dashed dotted line) and the Alford fit (blue dotted line). The constraints on the lower limit of the maximum mass from the revised Shapiro-delay based mass measurement on the massive pulsar PSR J0740+6620 [33] are shown with 1σ and 2σ precision. Additionally, we mark the excluded regions deduced from the gravitational wave observation GW170817 [64, 65].

functional fit provided in this work allows to interpret the parameters of the CSS model that are favorable for explaining NS phenomenology in terms of the unknown coupling constants of the effective low-energy QCD Lagrangian. We have also tried to fit the nlNJL EoS with

the Alford parameterization, but this resulted in a worse quality of the fit when compared to the CSS one, at least for masses well below the maximum mass. Therefore, we could confirm for the first time that the covariant nlNJL is fitted to the CSS parameterization with high accuracy. While these microphysical parameters, the diquark coupling and the vector meson coupling considered here to vary in the range of $0.7 < \eta_D < 0.8$ and $0.11 < \eta_V < 0.18$, respectively, it is possible to extend the range of applicability of the CSS parameter fit also beyond these ranges.

Our studies can be used not only in order to explore the phase transition between hadronic and color superconducting quark matter in cold NS, but it can also be extended to finite temperatures when it will be useful in simulations of core collapse supernovae [68] and neutron star mergers [69–71] involving quark matter deconfinement.

ACKNOWLEDGMENTS

SA acknowledges the COST Action CA16214 “PHAROS” for the support of this project through the Short Term Scientific Mission (STSM), and appreciates the hospitality of the Physics Department of Faculty of Science at University of Zagreb for having her as a guest scientist. This work has been supported in part by the Polish National Science Centre (NCN) under grant No. 2019/33/B/ST9/03059 (SA,DB,MS), by the Russian Fund for Basic Research (RFBR) under grant No. 18-02-40137 (DB) and Consejo Nacional de Investigaciones Científicas y Técnicas, under Grant No. PIP17-700 (AGG).

-
- [1] E. Annala, T. Gorda, A. Kurkela, J. Nättilä, and A. Vuorinen, *Nature Phys.* **16**, 907 (2020), arXiv:1903.09121 [astro-ph.HE].
 - [2] D. Blaschke, A. Ayriyan, D. E. Alvarez-Castillo, and H. Grigorian, *Universe* **6**, 81 (2020), arXiv:2005.02759 [astro-ph.HE].
 - [3] Y. Nambu and G. Jona-Lasinio, *Phys. Rev.* **122**, 345 (1961).
 - [4] Y. Nambu and G. Jona-Lasinio, *Phys. Rev.* **124**, 246 (1961).
 - [5] T. Eguchi, *Phys. Rev. D* **14**, 2755 (1976).
 - [6] M. K. Volkov, *Annals Phys.* **157**, 282 (1984).
 - [7] U. Vogl, M. F. M. Lutz, S. Klimt, and W. Weise, *Nucl. Phys. A* **516**, 469 (1990).
 - [8] S. Klimt, M. F. M. Lutz, U. Vogl, and W. Weise, *Nucl. Phys. A* **516**, 429 (1990).
 - [9] S. P. Klevansky, *Rev. Mod. Phys.* **64**, 649 (1992).
 - [10] D. Ebert, H. Reinhardt, and M. K. Volkov, *Prog. Part. Nucl. Phys.* **33**, 1 (1994).
 - [11] T. Hatsuda and T. Kunihiro, *Phys. Rept.* **247**, 221 (1994), arXiv:hep-ph/9401310.
 - [12] M. Buballa, *Phys. Rept.* **407**, 205 (2005), arXiv:hep-ph/0402234.
 - [13] H. Kleinert, in *14th International School of Subnuclear Physics: Understanding the Fundamental Constituents of Matter* (1976).

- [14] D. Ebert and V. N. Pervushin, in *18th International Conference on High-Energy Physics* (1976).
- [15] R. T. Cahill and C. D. Roberts, Phys. Rev. D **32**, 2419 (1985).
- [16] V. N. Pervushin, Y. L. Kalinovsky, W. Kallies, and N. A. Sarikov, Fortsch. Phys. **38**, 334 (1990).
- [17] S. M. Schmidt, D. Blaschke, and Y. L. Kalinovsky, Phys. Rev. C **50**, 435 (1994).
- [18] R. D. Bowler and M. C. Birse, Nucl. Phys. A **582**, 655 (1995), arXiv:hep-ph/9407336.
- [19] G. Ripka, *Quarks bound by chiral fields: The quark-structure of the vacuum and of light mesons and baryons* (1997).
- [20] C. J. Burden, L. Qian, P. C. Tandy, C. D. Roberts, and M. J. Thomson, Nucl. Phys. B Proc. Suppl. **47**, 362 (1996).
- [21] D. Blaschke, G. Burau, Y. L. Kalinovsky, P. Maris, and P. C. Tandy, Int. J. Mod. Phys. A **16**, 2267 (2001), arXiv:nucl-th/0002024.
- [22] H. T. Ding *et al.*, Phys. Rev. Lett. **123**, 062002 (2019), arXiv:1903.04801 [hep-lat].
- [23] C. Ratti, M. A. Thaler, and W. Weise, Phys. Rev. D **73**, 014019 (2006), arXiv:hep-ph/0506234.
- [24] D. Horvatic, D. Blaschke, D. Klabucar, and O. Kaczmarek, Phys. Rev. D **84**, 016005 (2011), arXiv:1012.2113 [hep-ph].
- [25] A. E. Radzhabov, D. Blaschke, M. Buballa, and M. K. Volkov, Phys. Rev. D **83**, 116004 (2011), arXiv:1012.0664 [hep-ph].
- [26] S. Benic, D. Blaschke, and M. Buballa, Phys. Rev. D **86**, 074002 (2012), arXiv:1206.6582 [hep-ph].
- [27] S. Noguera and N. N. Scoccola, Phys. Rev. D **78**, 114002 (2008), arXiv:0806.0818 [hep-ph].
- [28] G. A. Contrera, A. G. Grunfeld, and D. B. Blaschke, Phys. Part. Nucl. Lett. **11**, 342 (2014), arXiv:1207.4890 [hep-ph].
- [29] G. A. Contrera, A. G. Grunfeld, and D. Blaschke, Eur. Phys. J. A **52**, 231 (2016), arXiv:1605.08430 [hep-ph].
- [30] P. Senger (CBM), Phys. Scripta **96**, 054002 (2021), arXiv:2102.08908 [nucl-ex].
- [31] D. G. Dumm, J. P. Carlomagno, and N. N. Scoccola, Symmetry **13**, 121 (2021), arXiv:2101.09574 [hep-ph].
- [32] C. Gocke, D. Blaschke, A. Khalatyan, and H. Grigorian, in *Workshop on Quark Matter in Astrophysics and Particle Physics* (2001) arXiv:hep-ph/0104183.
- [33] E. Fonseca *et al.*, (2021), arXiv:2104.00880 [astro-ph.HE].
- [34] T. Klähn and T. Fischer, Astrophys. J. **810**, 134 (2015), arXiv:1503.07442 [nucl-th].
- [35] T. Klähn, D. Blaschke, F. Sandin, C. Fuchs, A. Faessler, H. Grigorian, G. Röpke, and J. Trümper, Phys. Lett. B **654**, 170 (2007), arXiv:nucl-th/0609067.
- [36] T. Klähn, R. Lastowiecki, and D. B. Blaschke, Phys. Rev. **D88**, 085001 (2013), arXiv:1307.6996 [nucl-th].
- [37] D. Gomez Dumm, D. B. Blaschke, A. G. Grunfeld, and N. N. Scoccola, Phys. Rev. D **73**, 114019 (2006), arXiv:hep-ph/0512218.
- [38] D. B. Blaschke, D. Gomez Dumm, A. G. Grunfeld, T. Klähn, and N. N. Scoccola, Phys. Rev. C **75**, 065804 (2007), arXiv:nucl-th/0703088.
- [39] D. E. Alvarez-Castillo, D. B. Blaschke, A. G. Grunfeld, and V. P. Pagura, Phys. Rev. **D99**, 063010 (2019), arXiv:1805.04105 [hep-ph].
- [40] A. Ayriyan, D. Alvarez-Castillo, D. Blaschke, and H. Grigorian, Universe **5**, 61 (2019), arXiv:1812.10796 [astro-ph.HE].
- [41] M. A. R. Kaltenborn, N.-U. F. Bastian, and D. B. Blaschke, Phys. Rev. D **96**, 056024 (2017), arXiv:1701.04400 [astro-ph.HE].
- [42] M. Shahrbaaf, D. Blaschke, A. G. Grunfeld, and H. R. Moshfegh, Phys. Rev. C **101**, 025807 (2020), arXiv:1908.04740 [nucl-th].
- [43] M. Shahrbaaf, D. Blaschke, and S. Khanmohamadi, J. Phys. G **47**, 115201 (2020), arXiv:2004.14377 [nucl-th].
- [44] A. Ayriyan, D. Blaschke, A. G. Grunfeld, D. Alvarez-Castillo, H. Grigorian, and V. Abgaryan, “Bayesian analysis of multimessenger M-R data with interpolated hybrid EoS,” (2021), arXiv:2102.13485 [astro-ph.HE].
- [45] M. G. Alford, S. Han, and M. Prakash, Phys. Rev. D **88**, 083013 (2013), arXiv:1302.4732 [astro-ph.SR].
- [46] J. L. Zdunik and P. Haensel, Astron. Astrophys. **551**, A61 (2013), arXiv:1211.1231 [astro-ph.SR].
- [47] D. Blaschke and M. Cierniak, Astron. Nachr. **342**, 227 (2021), arXiv:2012.15785 [astro-ph.HE].
- [48] Z. Miao, A. Li, Z. Zhu, and S. Han, Astrophys. J. **904**, 103 (2020), arXiv:2006.00839 [nucl-th].
- [49] V. Paschalidis, K. Yagi, D. Alvarez-Castillo, D. B. Blaschke, and A. Sedrakian, Phys. Rev. D **97**, 084038 (2018), arXiv:1712.00451 [astro-ph.HE].
- [50] M. G. Alford and A. Sedrakian, Phys. Rev. Lett. **119**, 161104 (2017), arXiv:1706.01592 [astro-ph.HE].
- [51] J. J. Li, A. Sedrakian, and M. Alford, Phys. Rev. D **101**, 063022 (2020), arXiv:1911.00276 [astro-ph.HE].
- [52] D. Blaschke, S. Fredriksson, H. Grigorian, A. M. Oz-

- tas, and F. Sandin, Phys. Rev. D **72**, 065020 (2005), arXiv:hep-ph/0503194.
- [53] D. Blaschke, T. Klähn, R. Lastowiecki, and F. Sandin, J. Phys. G **37**, 094063 (2010), arXiv:1002.1299 [nucl-th].
- [54] M. Alford, M. Braby, M. W. Paris, and S. Reddy, Astrophys. J. **629**, 969 (2005), arXiv:nucl-th/0411016.
- [55] D. S. Zabolocki, D. B. Blaschke, R. Anglani, and Yu. L. Kalinovsky, *Three days of strong interactions. Proceedings, EMMI Workshop and 26th Max Born Symposium, Wroclaw, Poland, July 9-11, 2009*, Acta Phys. Polon. Supp. **3**, 771 (2010), arXiv:0912.4929 [hep-ph].
- [56] A. Ayriyan, D. Blaschke, A. G. Grunfeld, D. Alvarez-Castillo, H. Grigorian, and V. Abgaryan, (2021), arXiv:2102.13485 [astro-ph.HE].
- [57] H. T. Cromartie *et al.* (NANOGrav), Nature Astron. **4**, 72 (2019), arXiv:1904.06759 [astro-ph.HE].
- [58] B. K. Agrawal, Phys. Rev. D **81**, 023009 (2010), arXiv:1001.1584 [astro-ph.HE].
- [59] L. Bonanno and A. Sedrakian, Astron. Astrophys. **539**, A16 (2012), arXiv:1108.0559 [astro-ph.SR].
- [60] R. Lastowiecki, D. Blaschke, H. Grigorian, and S. Typel, Acta Phys. Polon. Supp. **5**, 535 (2012), arXiv:1112.6430 [nucl-th].
- [61] M. G. Alford, G. F. Burgio, S. Han, G. Taranto, and D. Zappalà, Phys. Rev. D **92**, 083002 (2015), arXiv:1501.07902 [nucl-th].
- [62] E. S. Fraga, R. D. Pisarski, and J. Schaffner-Bielich, Phys. Rev. D **63**, 121702 (2001), arXiv:hep-ph/0101143.
- [63] “NASA’s NICER Tests Matters Limits,” <https://svs.gsfc.nasa.gov/13832>, accessed: 2021-04-19.
- [64] A. Bauswein, O. Just, H.-T. Janka, and N. Stergioulas, Astrophys. J. Lett. **850**, L34 (2017), arXiv:1710.06843 [astro-ph.HE].
- [65] E. Annala, T. Gorda, A. Kurkela, and A. Vuorinen, Phys. Rev. Lett. **120**, 172703 (2018), arXiv:1711.02644 [astro-ph.HE].
- [66] S. Typel, G. Röpke, T. Klähn, D. Blaschke, and H. H. Wolter, Phys. Rev. C **81**, 015803 (2010), arXiv:0908.2344 [nucl-th].
- [67] S. Typel, Eur. Phys. J. A **52**, 16 (2016).
- [68] T. Fischer, N.-U. F. Bastian, M.-R. Wu, P. Baklanov, E. Sorokina, S. Blinnikov, S. Typel, T. Klähn, and D. B. Blaschke, Nature Astron. **2**, 980 (2018), arXiv:1712.08788 [astro-ph.HE].
- [69] A. Bauswein, N.-U. F. Bastian, D. B. Blaschke, K. Chatziioannou, J. A. Clark, T. Fischer, and M. Oertel, Phys. Rev. Lett. **122**, 061102 (2019), arXiv:1809.01116 [astro-ph.HE].
- [70] A. Bauswein, S. Blacker, V. Vijayan, N. Stergioulas, K. Chatziioannou, J. A. Clark, N.-U. F. Bastian, D. B. Blaschke, M. Cierniak, and T. Fischer, Phys. Rev. Lett. **125**, 141103 (2020), arXiv:2004.00846 [astro-ph.HE].
- [71] S. Blacker, N.-U. F. Bastian, A. Bauswein, D. B. Blaschke, T. Fischer, M. Oertel, T. Soultanis, and S. Typel, Phys. Rev. D **102**, 123023 (2020), arXiv:2006.03789 [astro-ph.HE].